SAPIENZA
UNIVERSITÀ DI ROMA

KIDs for W band in Italy

Alessandro Paiella

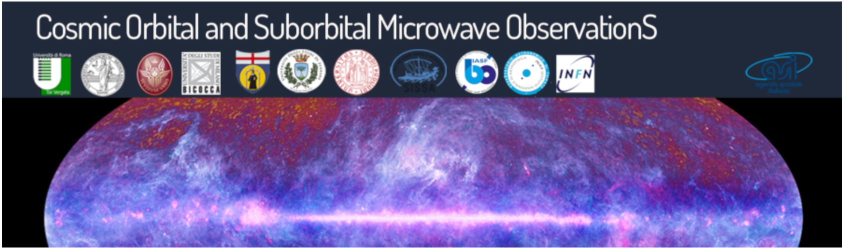

4[th] ASI/COSMOS Workshop: Ground–based CMB experiments

Dipartimento di Fisica – Università degli Studi di Milano
4[th]–5[th] March 2019

Kinetic Inductance Detectors

- Kinetic Inductance Detectors (KIDs) are superconductive detectors, where the radiation is detected by sensing changes of the kinetic inductance, L_k.
- A superconductor, cooled below its critical temperature T_c, presents two populations of electrons: quasiparticles and Cooper pairs (binding energy 2Δ).
- Pair-breaking radiation ($h\nu > 2\Delta$), absorbed in a superconducting film, breaks Cooper pairs, producing a change in the population relative densities, and thus in L_k.
- In the lumped element configuration, a superconducting strip is properly shaped and sized in order to perform like a radiation absorber.
- This structure, which is an inductor as well, is coupled to a capacitor to form a high–Q resonator.

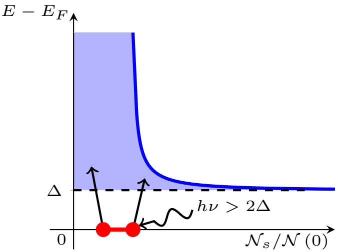

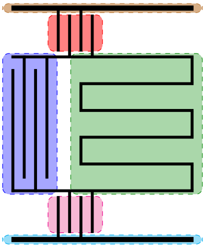

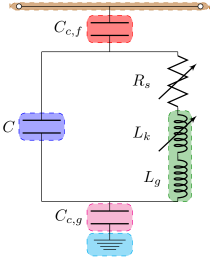

Kinetic Inductance Detectors
Working principle

- The change in L_k produces a change in the resonant frequency, ν_r, and in the quality factor, Q.
- They can be sensed by measuring the change in the amplitude and phase of the bias signal of the resonator, transmitted past the resonator through a feedline.
- KID design and readout scheme are intrinsically multiplexable for large–format arrays.

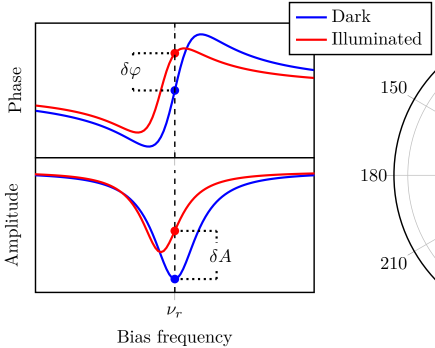

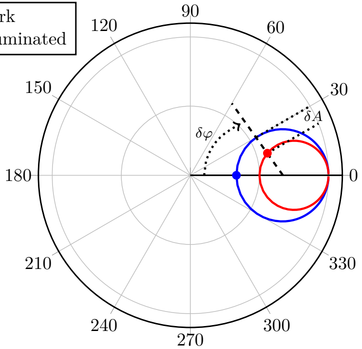

Kinetic Inductance Detectors
Working principle

- The change in L_k produces a change in the resonant frequency, ν_r, and in the quality factor, Q.
- They can be sensed by measuring the change in the amplitude and phase of the bias signal of the resonator, transmitted past the resonator through a feedline.
- KID design and readout scheme are intrinsically multiplexable for large–format arrays.

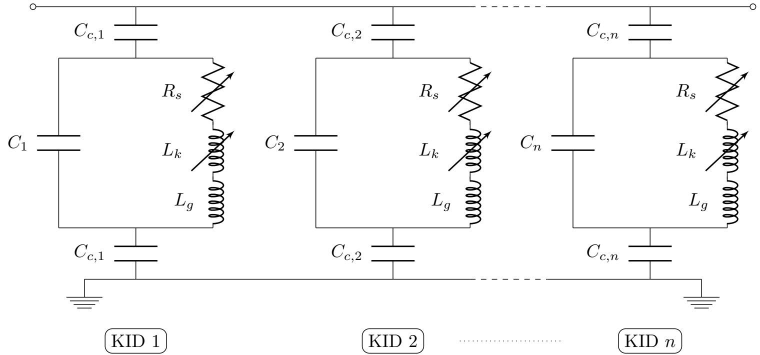

Astrophysics in the W–Band

- W–band: [75, 110] GHz.
- This band lies at an interesting transition between frequencies where Galactic emission is dominated by free–free, synchrotron and spinning dust, and frequencies where is dominated by thermal dust.

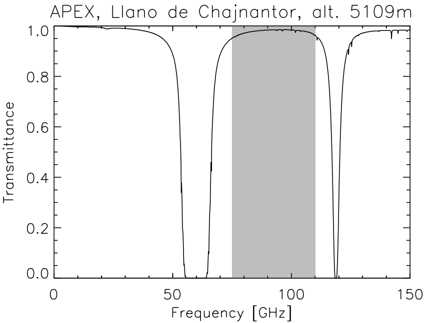

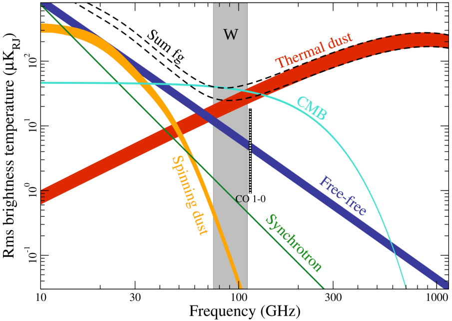

- In the W–band, the atmosphere is quite transparent, and then we can perform ground–based observations, avoiding the costs, complications and aperture limitations of balloon–borne and space–based missions.

Ground–based W–band

Science in W–band

- CMB polarisation → STRIP2 see C. Franceschet talk;
- Spectral distortions → COSMO see P. de Bernardis talk;
- Sunyaev–Zel'dovich effect → SRT see A. Navarrini talk.

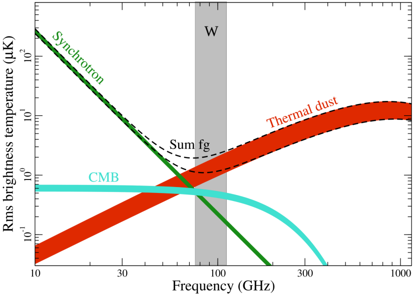

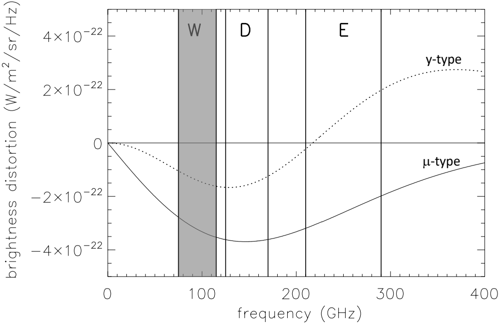

Sardinia Radio Telescope

- 64 m primary mirror;
- 7.9 m secondary mirror;
- pointing accuracy of 2–5 arcsec.

Search for the superconductive material (*Paiella A. et al. 2016, JLTP*)

- W–band: [75, 110] GHz
- $h\nu > 2\Delta = 3.52\, k_B\, T_c \Rightarrow T_c < 1.02\,\mathrm{K}$
- Aluminum

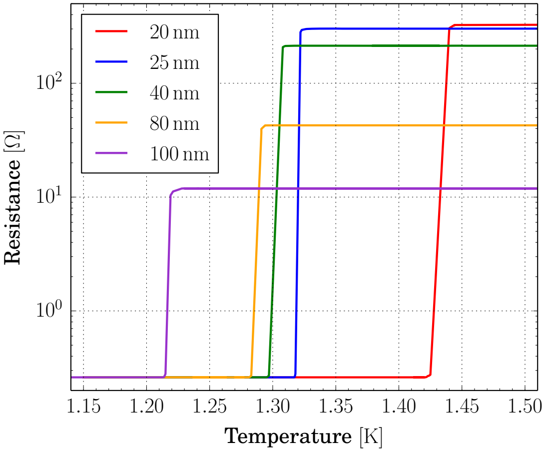

Search for the superconductive material (*Paiella A. et al. 2016, JLTP*)

- W–band: [75, 110] GHz
- $h\nu > 2\Delta = 3.52\, k_B\, T_c \Rightarrow T_c < 1.02\,\mathrm{K}$
- Aluminum

40 nm thick

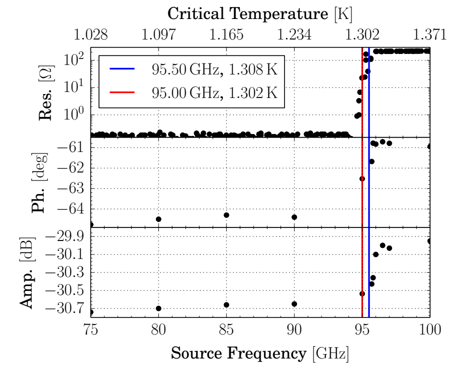

80 nm thick

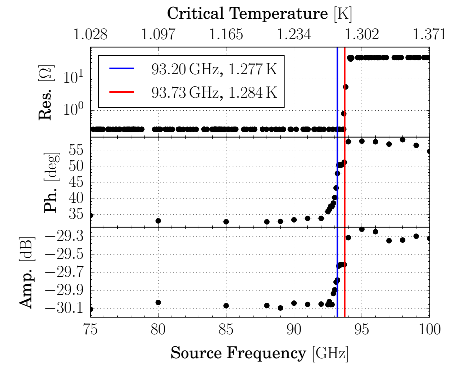

Search for the superconductive material (*Paiella A. et al. 2016, JLTP*)

- W–band: [75, 110] GHz
- $h\nu > 2\Delta = 3.52\, k_B\, T_c \Rightarrow T_c < 1.02\,\mathrm{K}$
- Titanium–Aluminum bilayer (*Catalano A. et al. 2016, A&A*)

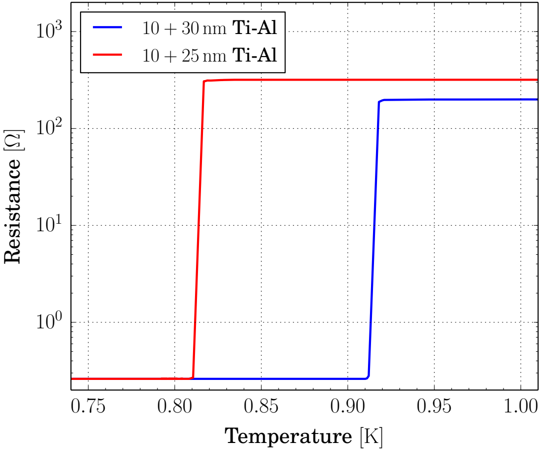

Search for the superconductive material (*Paiella A. et al. 2016, JLTP*)

- W–band: [75, 110] GHz
- $h\nu > 2\Delta = 3.52\, k_B\, T_c \Rightarrow T_c < 1.02\,\mathrm{K}$
- Titanium–Aluminum bilayer (*Catalano A. et al. 2016, A&A*)

$10 + 25$ nm thick

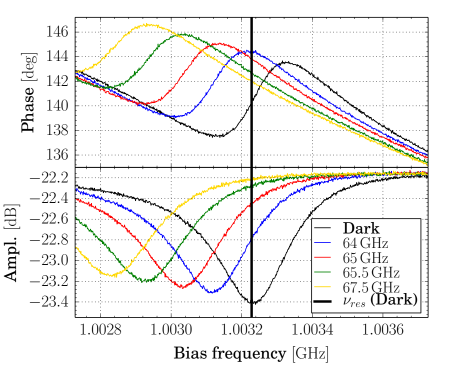

$10 + 30$ nm thick

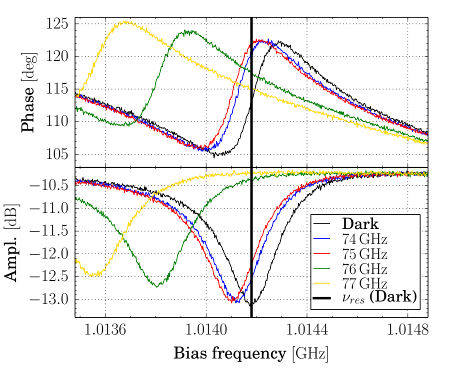

Properties & Performance

Configuration

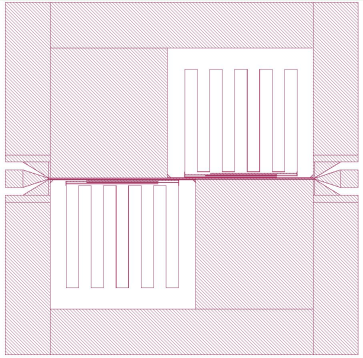

- CPW feedline;
- back illumination;
- no radiation coupler;
- no $\lambda/4$ backshort;
- basic optimisation.

Material Properties

t [nm]	T_c [mK]	$\Delta(0)$ [meV]	$R_\square$ [$\Omega/\square$]	$L_\square$ [pH/$\square$]
$10+25$	812	0.124	0.952	1.62
$10+30$	914	0.138	0.635	0.962

Electrical Performance @150 mK

t [nm]	Q_i	Q_c	Q
$10+25$	3.0×10^4	2.2×10^4	1.3×10^4
$10+30$	3.2×10^4	2.5×10^4	1.4×10^4

Optical Performance @150 mK

t [nm]	ν_{co} [GHz]	NEP $\left[\mathrm{fW}/\sqrt{\mathrm{Hz}}\right]$	$\mathrm{NET_{RJ}}$ $\left[\mathrm{mK}\sqrt{\mathrm{s}}\right]$
$10+25$	64	3.9	2.8
$10+30$	74	5.8	4.2

Fabrication

- The detector arrays are fabricated in the ISO5/ISO6 clean room of IFN–CNR in Rome.
- Substate: high–quality (FZ method) intrinsic Si(100) wafers, with high resistivity ($\rho > 10\,\mathrm{k\Omega\,cm}$), double side polished (diameter 2, 3, and 4″).
- Fabrication process (*Colantoni I. et al 2016, JLTP*):

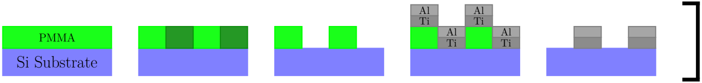

Uniform deposition of PMMA on Si substrate

Electron–Beam Litography

Development in a solution (1:1) of MIBK and IPA

Electron–gun evaporation

Lift–off

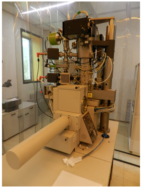

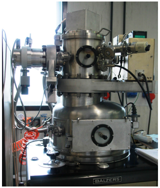

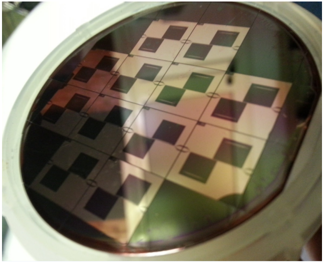

CNR IFN
Istituto di Fotonica e Nanotecnologie

KID design & simulations
Optical simulations

What do they constrain?

- material and thickness of superconducting film ($\Rightarrow L_k$) and dielectric substrate;
- geometry and size of absorber ($\Rightarrow L_g$) and radiation couplers, number of detectors;
- illumination configuration.

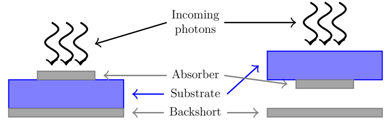

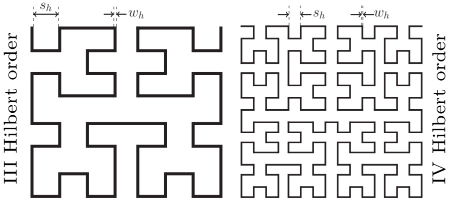

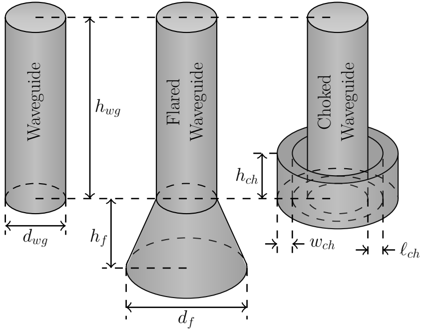

Parameters

	Geometrical	Electrical
Waveguide	h_{wg}, d_{wg}	
Flare	h_f, d_f	
Choke	h_{ch}, w_{ch}, ℓ	
Absorber (Ti–Al)	geom., s_h, w_h, t	L_k, L_g
Substrate (Si)	d	
Illumination	front, back	
vacuum/backshort	d_b	

KID design & simulations

Optical simulation results

HFSS

Design: radiation coupler + absorber + substrate + backshort

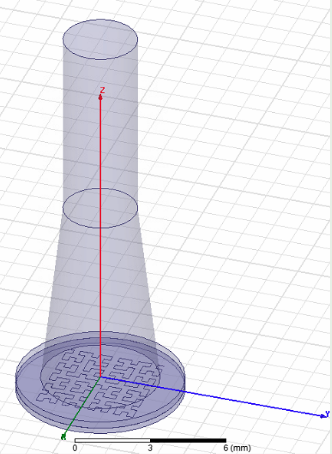

Results

Hilbert	Radiation Coupler	Absor.	Losses
III	waveguide	81%	< 2%
	flared waveguide	81%	< 2%
	choked waveguide	83%	< 1.5%
IV	waveguide	90%	< 1%
	flared waveguide	91%	< 1%
	choked waveguide	91%	< 0.5%

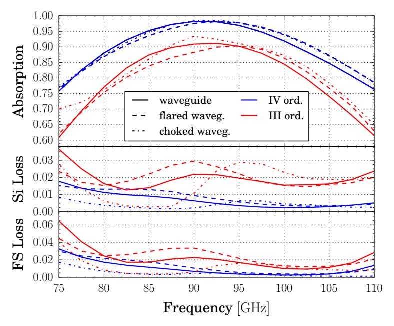

KID design & simulations
Optical simulation results

HFSS

Excitation: two modes, mimicking both polarisations of the incident radiation

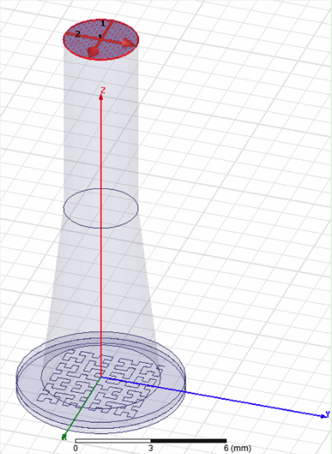

Results

Hilbert	Radiation Coupler	Absor.	Losses
III	waveguide	81%	$< 2\%$
	flared waveguide	81%	$< 2\%$
	choked waveguide	83%	$< 1.5\%$
IV	waveguide	90%	$< 1\%$
	flared waveguide	91%	$< 1\%$
	choked waveguide	91%	$< 0.5\%$

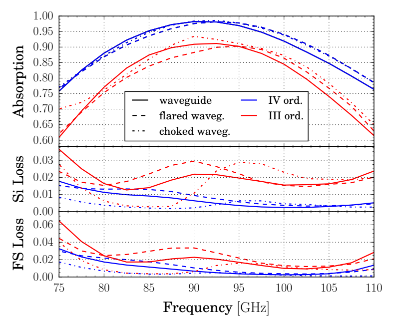

KID design & simulations

Optical simulation results

HFSS

Boundary: impedance of free–space

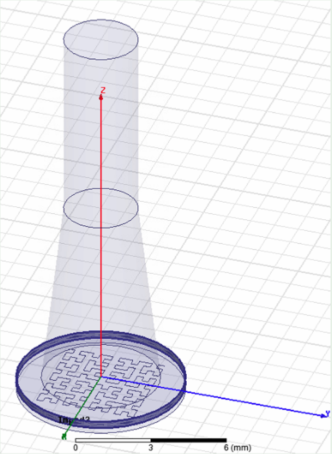

Results

Hilbert	Radiation Coupler	Absor.	Losses
III	waveguide	81%	$< 2\%$
	flared waveguide	81%	$< 2\%$
	choked waveguide	83%	$< 1.5\%$
IV	waveguide	90%	$< 1\%$
	flared waveguide	91%	$< 1\%$
	choked waveguide	91%	$< 0.5\%$

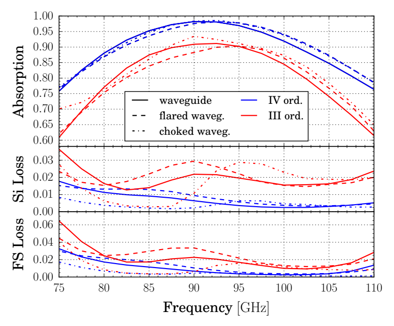

KID design & simulations
Optical simulation results

HFSS

Boundary: impedance of the substrate

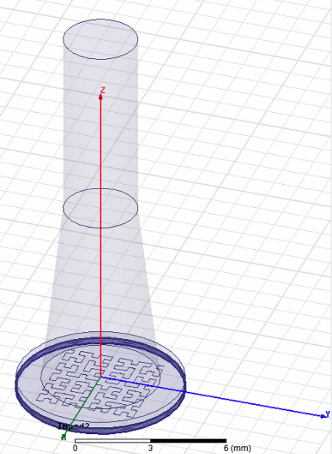

Results

Hilbert	Radiation Coupler	Absor.	Losses
III	waveguide	81%	$< 2\%$
	flared waveguide	81%	$< 2\%$
	choked waveguide	83%	$< 1.5\%$
IV	waveguide	90%	$< 1\%$
	flared waveguide	91%	$< 1\%$
	choked waveguide	91%	$< 0.5\%$

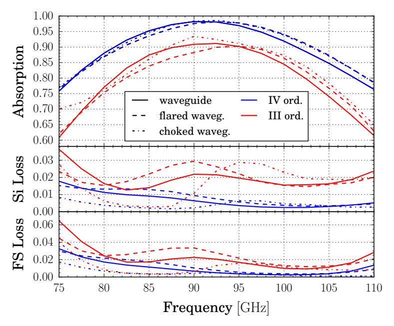

KID design & simulations

Optical simulation results

HFSS

Boundary: sheet resistance of the Ti–Al bilayer 10+25 nm thick

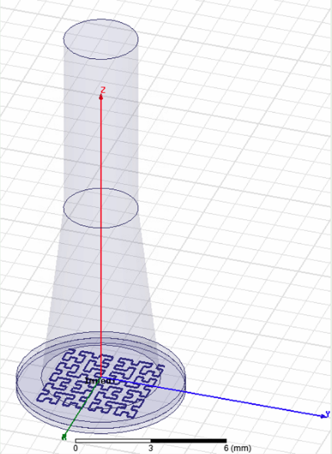

Results

Hilbert	Radiation Coupler	Absor.	Losses
III	waveguide	81%	< 2%
	flared waveguide	81%	< 2%
	choked waveguide	83%	< 1.5%
IV	waveguide	90%	< 1%
	flared waveguide	91%	< 1%
	choked waveguide	91%	< 0.5%

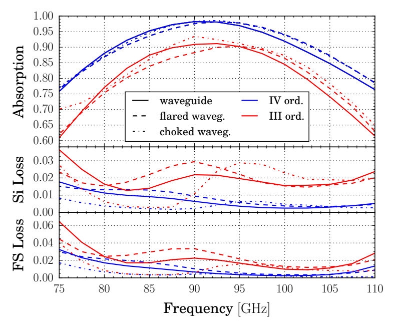

Optical simulation reliability
The OLIMPO case (*Paiella A. et al. 2019, JCAP*)

- For the OLIMPO KIDs, the same optimisation procedure has been used, as an example:
  - 150 GHz receiver: front illuminated IV order Hilbert absorber coupled to the radiation via single–mode waveguide;
  - 350 GHz receiver: front illuminated IV order Hilbert absorber coupled to the radiation via single–mode flared waveguide.

150 GHz receiver

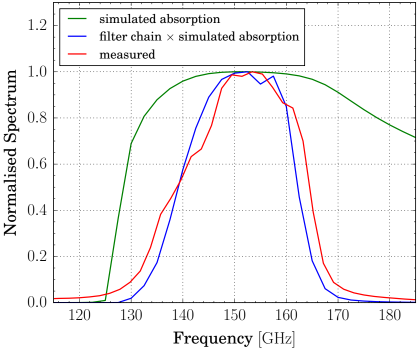

350 GHz receiver

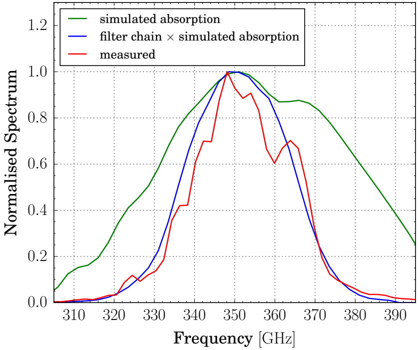

Maximise the responsivity

Responsivity: III vs. IV Hilbert order

$$\mathcal{R}_{opt} = \eta_{opt}\mathcal{R}_{elec} = -\eta_{opt}\frac{\eta_{pb}\tau_{qp}}{\Delta}4Q\frac{\delta x}{\delta N_{qp}}$$

$$\propto \eta_{opt}\frac{QL_k}{VL}$$

$$\mathcal{R}^{max}_{opt} \propto \eta_{opt}\frac{Q_i L_k}{VL} \propto \frac{L_\Box}{\rho}\frac{\eta_{opt}}{\ell^{tot}_{abs} w_h}\frac{1}{\sqrt{LC}}$$

$$\frac{\mathcal{R}^{\mathrm{III}}_{opt}}{\mathcal{R}^{\mathrm{IV}}_{opt}} = \frac{\eta^{\mathrm{III}}_{opt}}{\eta^{\mathrm{IV}}_{opt}}\frac{\ell^{tot,\mathrm{IV}}_{abs}}{\ell^{tot,\mathrm{III}}_{abs}}\underbrace{\sqrt{\frac{L^{\mathrm{IV}}C^{\mathrm{IV}}}{L^{\mathrm{III}}C^{\mathrm{III}}}}}_{\text{lumped element condition}}$$

$$\propto \frac{\eta^{\mathrm{III}}_{opt}}{\eta^{\mathrm{IV}}_{opt}}\left(\frac{\ell^{tot,\mathrm{IV}}_{abs}}{\ell^{tot,\mathrm{III}}_{abs}}\right)^2 \sim 5.5 \Rightarrow \mathrm{III}$$

Hilbert	s_h [μm]	w_h [μm]	ℓ^{tot}_{abs} [μm]
III	450	2	28413
IV	270	2	69105

Lumped Element Condition

- How: $\ell^{tot}_{abs} \ll \lambda_r$.
- Why: voltage and current do not vary over the physical dimension of the elements $\Rightarrow$ uniform radiation absorption in the inductor.
- Operatively: current distribution null in the capacitor and uniform in the inductor.

Example:

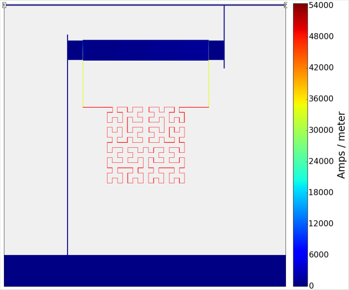

Last Pixel of 150 GHz array

$\ell^{tot}_{abs} = 41310\,\mu\mathrm{m},\ \lambda_r \sim 1.2\,\mathrm{m}\ \ (\nu_r \sim 240\,\mathrm{MHz})$

On–going activity

Completing the KID design via electrical simulations

What do they constrain?

- geometry and size of feedline and capacitors;
- coupling between resonators and feedline.

Parameters

	Geometrical	Electrical	
Feedline	w_{fl}	Z_{fl}	
Capacitor	$\ell_c,\ w_c,\ s_c$	C	$\Leftarrow \nu_r$ $\Rightarrow Q_i$
Coupling Capacitor	$\ell_{cc},\ w_{cc},\ s_{cc}$	C_c	$\Leftarrow Q_c$

$$\nu_r = \frac{1}{2\pi\sqrt{LC}} \sim 350\,\mathrm{MHz} \ \text{ by LE condition}$$

$$\left.\begin{aligned} Q_i &= \frac{1}{R_s}\sqrt{\frac{L}{C}} \sim 10^4 - 10^5 \\ Q_c &= \frac{8C}{2\pi\nu_r C_c^2 Z_{fl}} \sim Q_i \end{aligned}\right\} \Rightarrow Q, \mathcal{R} \text{ maximised}$$

$$L = L_k + L_g \ \text{ by optical simulations}$$

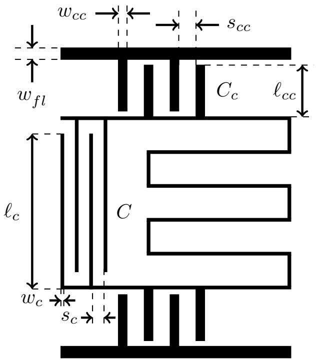

SONNET simulations

- Input: resonator & feedline design;
- Output:
  - feedline impedance (Z_{fl});
  - scattering parameters (S);
  - current distribution.

On–going activity
Working Temperature

$$\mathrm{NET}\left(P_{\mathrm{bkg}}, T\right) = \sqrt{\left[\mathrm{NET}_{\mathrm{phot}}\left(P_{\mathrm{bkg}}\right)\right]^2 + \left[\mathrm{NET}_{\mathrm{gr}}\left(P_{\mathrm{bkg}}, T\right)\right]^2}$$

Ingredients

- $T_c = 812\,\mathrm{mK}$ measured for 10+25 Ti–Al;
- $\ell_{tot}^{abs} = 28\,413\,\mu\mathrm{m}$, $w_h = 2\,\mu\mathrm{m}$;
- $\eta_{opt}(\nu)$ simulated.

NET vs. T for different PWV values

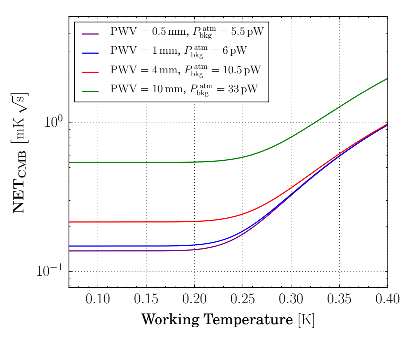

NET vs. P_{bkg}, T

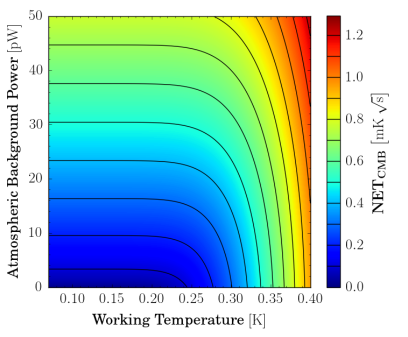

On–going activity
Working Temperature

$$\mathrm{NET}\left(P_{\mathrm{bkg}}, T\right) = \sqrt{\left[\mathrm{NET}_{\mathrm{phot}}\left(P_{\mathrm{bkg}}\right)\right]^2 + \left[\mathrm{NET}_{\mathrm{gr}}\left(P_{\mathrm{bkg}}, T\right)\right]^2}$$

Ingredients

- $T_c = 812\,\mathrm{mK}$ measured for 10+25 Ti–Al;
- $\ell_{tot}^{abs} = 28\,413\,\mu\mathrm{m}$, $w_h = 2\,\mu\mathrm{m}$;
- $\eta_{opt}(\nu)$ simulated.

$\mathrm{NET}_{\mathrm{gr}}$ vs. $\mathrm{NET}_{\mathrm{phot}}$

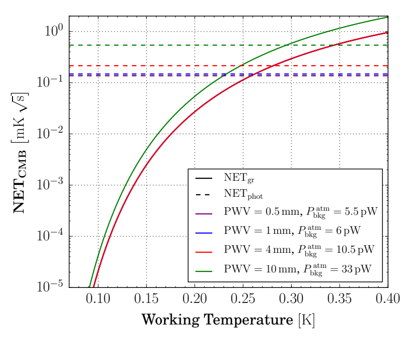

NET vs. P_{bkg}, T

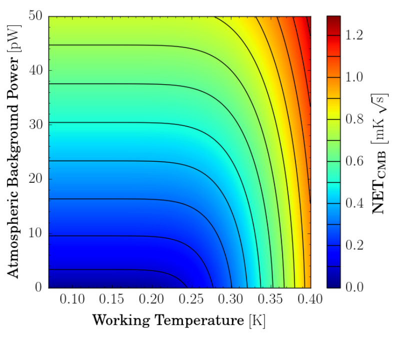

On–going activity

Possible Integration in a mm–wave ground–based telescope

Advantages of this optical system and detectors

- Cope with large radiative loading with efficient filters stack;
- control straylight with internal reimaging optics;
- edge-taper controlled via feedhorns and cold stop;
- wide correct focal plane;
- mechanical cooler for continuous operation;
- sub–K cooler can be 0.25 K (NET calculations seen above).